ADVANCES IN ATMOSPHERIC SCIENCES, VOL. 34, MARCH 2017, 397–410

• **Original Paper** •

Influence of Island Chains on the Kuroshio Intrusion in the Luzon Strait

Zhida HUANG[1], Hailong LIU[*2,3], Pengfei LIN[2], and Jianyu HU[1]

[1]*State Key Laboratory of Marine Environmental Science, College of Ocean and Earth Sciences, Xiamen University, Xiamen* 361102, *China*

[2]*State Key Laboratory of Numerical Modeling for Atmospheric Sciences and Geophysical Fluid Dynamics, Institute of Atmospheric Physics, Chinese Academy of Sciences, Beijing* 100029, *China*

[3]*College of Earth Sciences, University of Chinese Academy of Sciences, Beijing* 100049, *China*

(Received 15 June 2016; revised 21 August 2016; accepted 2 September 2016)

ABSTRACT

By applying a global high-resolution (0.1°) OGCM, the influence of the island chains in the Luzon Strait (LS) on the Kuroshio intrusion is studied systematically. The island chains in the LS are separated into three parts: the south island chain, the middle and north island chain, and Babuyan Island. One control and three sensitivity experiments are conducted by adding these three parts of the topography gradually. From comparisons of the circulation, temperature, and salinity structures, it is found that the south island chain decreases the westward bending of the main Kuroshio path, the middle and north island chain increases the westward bending, and Babuyan Island also increases the westward bending. These results are extremely clear in winter. Dynamic diagnoses suggest that the westward bending increases with an increase in the incidence angle of the Kuroshio and an increase in the Kuroshio east branch transport. Moreover, the middle and north island chain can split the Kuroshio into two parts, the Kuroshio west and east branches, which can be seen clearly in the satellite altimeter maps.

Key words: Luzon Strait, Kuroshio intrusion, island chains, Kuroshio east branch

Citation: Huang, Z. D., H. L. Liu, P. F. Lin, and J. Y. Hu, 2017: Influence of island chains on the Kuroshio intrusion in the Luzon Strait. *Adv. Atmos. Sci.*, **34**(3), 397–410, doi:10.1007/s00376-016-6159-y.

1. Introduction

The Luzon Strait (LS) is the key channel for water exchange between the South China Sea (SCS) and the Northwest Pacific (NWP). The Kuroshio intrudes the Northeast SCS through the LS, with strong intrusion in winter and weak intrusion in summer (e.g., Lan et al., 2004; Hu et al., 2011; Nan et al., 2014). Understanding of the dynamics of the Kuroshio intrusion has gradually progressed with increasing observations, but how the Kuroshio intrudes into the SCS is still under debate (Hu et al., 2000, 2011). Research on the Kuroshio intrusion mainly includes three aspects: intrusion types (e.g., Li et al., 1998; Caruso et al., 2006; Nan et al., 2014; Huang et al., 2016), water exchange in the LS (e.g., Lan et al., 2004; Tian et al., 2006; Shu et al., 2014), and the interactions between the Kuroshio and mesoscale processes (e.g., Zheng et al., 2011; Hu et al., 2012; Lu and Liu, 2013). Based on satellite altimeter data, Caruso et al. (2006) depicted five types of Kuroshio intrusion paths, including the Kuroshio SCS branch, the Kuroshio loop, the detached anticyclonic eddy, the cyclonic intrusion, and the leaping path. Recently, Huang et al. (2016) proposed a Double-Index method to classify Kuroshio paths and summarized these five types into three typical patterns, including the Kuroshio Warm Eddy Path (KWEP), Kuroshio Cold Eddy Path (KCEP), and leaking path. According to *in-situ* observation in October 2005, Tian et al. (2006) confirmed that the Luzon Strait Transport (LST) has a sandwiched vertical structure, which is supported by several models and observations (Nan et al., 2014; Shu et al., 2014). Zheng et al. (2011) revealed that nonlinear Rossby eddies can propagate into the SCS from analyses of satellite altimeter data. Furthermore, Hu et al. (2012) provided evidence for the nonlinear Rossby eddies entering the SCS through in-situ observation in January 2010.

The land–sea boundary is complicated in the LS (Figs. 1a and c). Numerous islands exist between Taiwan Island and Luzon Island, mainly including the Babuyan Island chain in the south (including the islands of Fuga, Camiguin, Dalupiri, Calayan, and Babuyan), the Batan island chain in the middle (including the islands of Sabtang, Batan, and Itbayat), and Lan-Yü and Lü islands in the north. Previous studies have indicated that these islands play important roles in the Kuroshio intrusion in the LS. Combining Advanced Synthetic Aperture Radar with Argos satellite-tracked surface drifter data, Zheng et al. (2008) found that the Karman vortex street occurs in

* Corresponding author: Hailong LIU
Email: lhl@lasg.iap.ac.cn

the wake of Babuyan Island. Results from numerical experiments suggest that these islands in the LS can dramatically influence the path of the Kuroshio intrusion (Metzger and Hurlburt, 2001; Lu and Liu, 2013). By using the 1/16° Naval Research Laboratory Layered Ocean Model, Metzger and Hurlburt (2001) revealed that the Calayan Bank can significantly decrease the westward bending of the main Kuroshio path in the LS. Therefore, less water from the Kuroshio will enter the SCS. Based on results from a 0.125° Hybrid Coordinate Ocean Model, Lu and Liu (2013) found that the sharp northeast cape of Luzon Island is one of the most important factors controlling the behavior of the Kuroshio entering or leaping the LS. However, the abovementioned studies mainly focused on the islands in the southern part of the LS (zone A in Fig. 1b). The effects of the islands in the middle and north LS (zone B in Fig. 1b) and Babuyan Island (zone C in Fig. 1b), which are situated along the main path of the Kuroshio, on the Kuroshio intrusion, have not been investigated to date.

In this study, we perform four numerical experiments to examine the effects of these islands on the Kuroshio intrusion using a quasi-global and high-resolution (0.1°) OGCM. Section 2 describes the observational data and numerical experi-

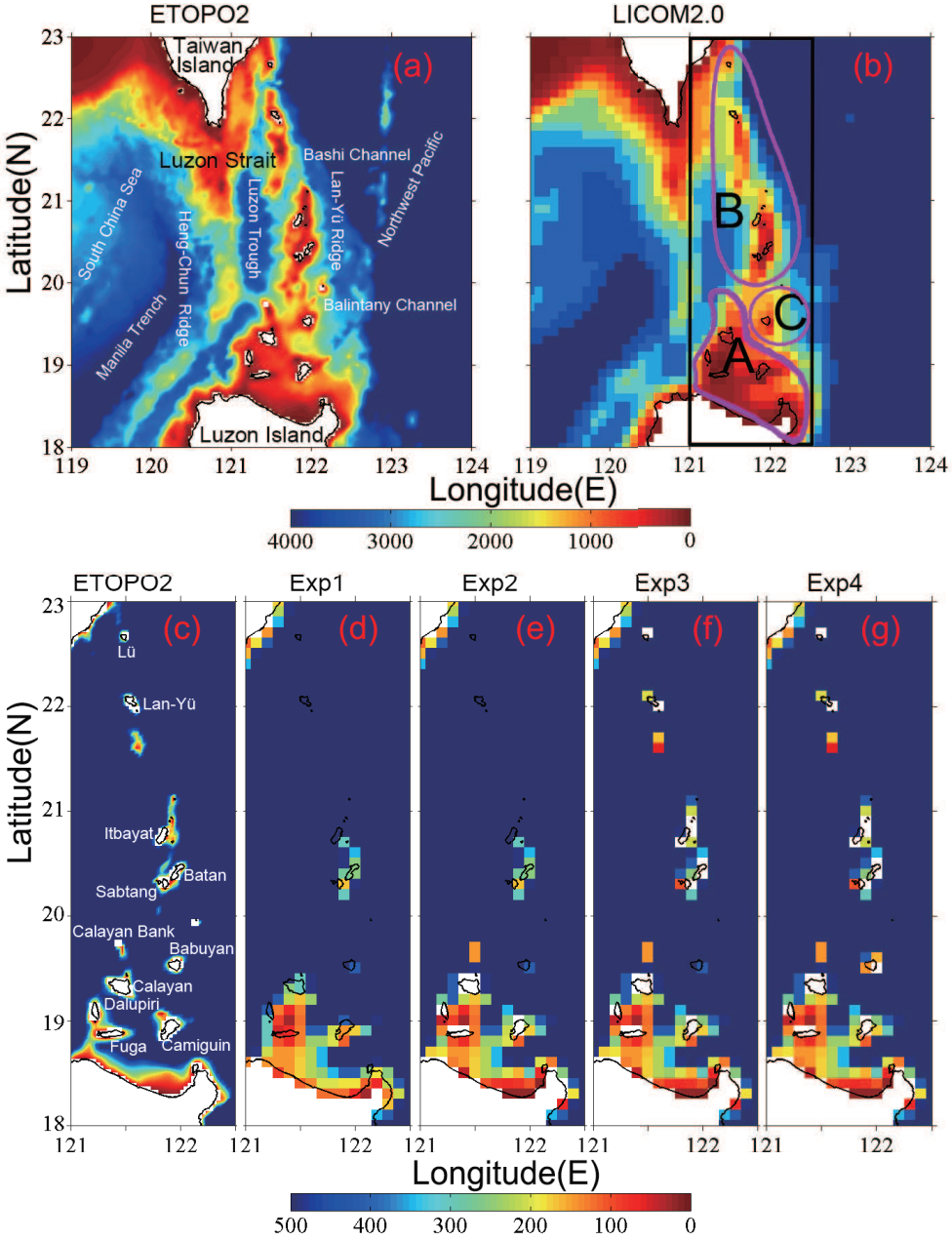

Fig. 1. Topography (units: m) around the Luzon Strait for (a) ETOPO2 and (b) LICOM2.0 interpolated from the DBDB5 dataset. Zones A, B, and C in the black box in panel (b) are the key regions for the present study. Panels (c) and (d–g) only present a water depth less than 500 m in the black box for ETOPO2 and the four experiments, respectively.

ments. Section 3 presents the change in sea surface currents, SST, and hydrographic section around the LS among the experiments, as well as comparisons between experiments and observations. Section 4 reports diagnostic analyses of the proportions of three Kuroshio intrusion types, the partitions of transport of the two Kuroshio branches, and the theoretical estimation of the Kuroshio's westward bending. Finally, the results of the study are summarized in section 5.

2. Observations and experiments

2.1. *Observations*

Three observational datasets are used in the present study. The merged satellite altimeter products during the period of 1993–2007, with a spatial resolution of 0.25°, obtained from the AVISO dataset (http://www.aviso.oceanobs.com), are used to assess the surface geostrophic currents in the LS. The remote sensing SST products, with a resolution of 0.25°, from 1993 to 2007, are from OISST (http://www.esrl.noaa.gov/psd/data/gridded/data.noaa.oisst.v2.highres.html). To examine temperature, salinity, and velocity along a specific section, we also use the objectively analyzed climatological temperature and salinity data from the World Ocean Atlas 2013 dataset (WOA13, http://www.nodc.noaa.gov/OC5/woa13/woa13data.html).

2.2. *Experiments*

A quasi-global OGCM, developed by the LASG/IAP, LICOM, is used to conduct all the numerical experiments in the present study (Liu et al., 2004, 2012). The high-resolution (1/10°) model is developed based on version 2.0 (Liu et al., 2012). The model's horizontal resolution has been increased from 1° to 0.1° and the vertical levels have been increased from 30 to 55. The simulation is forced by the daily dataset from CORE2 for the period 1948–2007. The detailed configurations of the high-resolution model can be found in Yu et al. (2012).

The model topography is derived from Digital Bathymetric Data Base 5 minute (DBDB5) of the Naval Oceanographic Office. The model topography does not present the island chains in the LS well because of the smoothed original data. Most islands are not exposed to the sea surface, as clearly evidenced by the differences between the model and the topography from the ETOPO2 dataset (Figs. 1a and b). Therefore, we separate these unexposed island chains into three groups: the island chain south of Babuyan Island, including the sharp northeast cape of Luzon Island, Zone A in Fig. 1b; the island chain north of Babuyan Island, Zone B in Fig. 1b; and Babuyan Island, Zone C in Fig. 1b. The names of islands in the LS are shown in Fig. 1c.

Figure 2 shows the climatological surface geostrophic currents (m s^{-1}) and the corresponding absolute dynamic topography (ADT, cm) around the LS for the satellite altimeter and LICOM2.0 simulation during 1993–2007. According to the patterns of currents, we choose the 115, 120, and 115 cm ADT contours (red dashed) to represent the main Kuroshio paths for the annual, summer (June), and winter (December) mean, respectively (Figs. 2a–c). Meanwhile, the 80, 85, and 70 cm SSH contours represent the main Kuroshio paths in LICOM2.0 (Figs. 2d–f).

The annual mean westward bending of the Kuroshio path in LICOM2.0 is much larger than that in AVISO (Figs. 2a and d). The large discrepancies mainly occur in winter when the Kuroshio intrusion becomes strong. LICOM2.0 shows a much more westward extending looping pattern (Figs. 2c and f). Additionally, results from observations indicate that parts of the Kuroshio water flow along the east side of the middle and north island chain, and this flow is named the Kuroshio east branch in the present study. However, no Kuroshio east branch exists in the LICOM2.0 simulation, and almost all Kuroshio water flows into the LS.

In this study, four experiments are carried out. Exp1 is the control run, and Exp2, Exp3, and Exp4 are designed by adding an island chain or island topography in zones A, B, and C (Fig. 1b) gradually, based on the ETOPO2 dataset. Details of the configurations of Exp1–Exp4 are listed in Table 1, and the corresponding model topography is shown in Figs. 1d–g. The four experiments are an integration of four years of daily CORE2 data. The last three years of outputs are used for analysis.

3. Results

3.1. *Surface geostrophic currents*

First, we examine the influences of island chains on the surface circulation patterns. Figures 3a–d show the annual mean SSH (cm) and the corresponding surface geostrophic currents (m s^{-1}) in Exp1–Exp4. Figures 3e–h and 3i–l are the results for summer and winter, respectively. The red dashed contours are also used to indicate the Kuroshio paths,

Table 1. Descriptions of the experiments in the present study. Zones A, B, and C are shown in Fig. 1b.

Name	Topography	Initial Condition	Forcing	Integration period
LICOM2.0	DBDB5	12-year spin-up	CORE2 from 1948 to 2007	60 years
Exp1 (Control run)	DBDB5	Last day of LICOM2.0 experiment	Daily Climatology of CORE2	4 years
Exp2	DBDB5 + Zone A	Last day of LICOM2.0 experiment	Daily Climatology of CORE2	4 years
Exp3	DBDB5 + Zone A + Zone B	Last day of LICOM2.0 experiment	Daily Climatology of CORE2	4 years
Exp4	DBDB5 + Zone A + Zone B + Zone C	Last day of LICOM2.0 experiment	Daily Climatology of CORE2	4 years

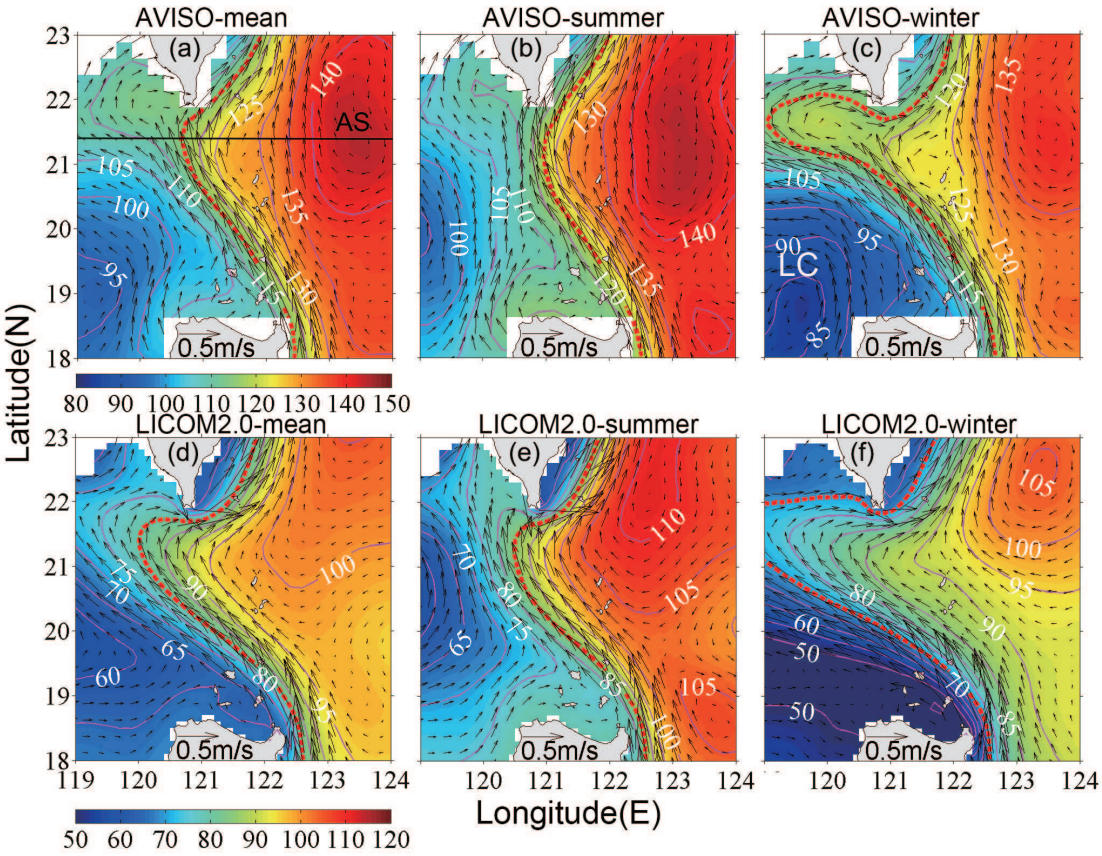

Fig. 2. Absolute dynamic topography (shaded; units: cm) and surface geostrophic currents (vectors; units: m s^{-1}) for the (a) annual, (b) summer, and (c) winter mean from the AVISO data during 1993–2007. Panels (d–f) are similar to (a–c) but for the results from LICOM2.0. The red dashed lines represent the Kuroshio paths in the LS. The black line AS (along 21.4°N from 119°E to 124°E) in panel (a) is the chosen section of velocity, temperature, and salinity for investigation. The LC in panel (c) denotes the active center where the Luzon cold eddy is located.

as in Fig. 2. Compared with the LICOM2.0 simulation during 1993–2007, the Kuroshio path for Exp1 tends to leap in summer and loop in winter. There is no significant distinction between Exp1 and the original experiment (Figs. 2d and 3a). These findings reflect the fact that a four-year integration can reproduce the mean features of the Kuroshio path of the original simulation and is appropriate for the present study.

After adding the south island chain, we find that the Kuroshio path in the annual mean (80 cm SSH contour) changes to a leaping state in Exp2 (Figs. 3a and b). In summer, the Kuroshio paths are in a leaping state for both Exp1 and Exp2. However, in winter, the looping path in Exp1 changes to a leaking path in Exp2, and part of the Kuroshio water leaps the LS and the rest of the water flows into the SCS. These results indicate that the southern island chain can decrease the westward bending of the Kuroshio path efficiently, particularly in winter when the looping path usually occurs.

When the middle and north island chain is further added again in Exp3, the Kuroshio splits into two parts by the island chain; namely, western and eastern branches (Figs. 3c, g and k). Therefore, two regions of large SSH gradient exist, which correspond to the two branches, with a region of relatively small SSH gradients between. Besides reducing the Kuroshio transport entering the LS, we also find that the middle and north island chain can also slightly increase the western bending of the Kuroshio path, especially in winter.

Babuyan Island is further added in Exp4. Compared with Exp3, Exp4 reveals a slightly larger westward bending of the Kuroshio path, as inferred from the 75 cm SSH contour (Figs. 3c and d), and this phenomenon mainly occurs in winter (Figs. 3h and l). In the annual mean, summer, or winter, the east branch of the Kuroshio is stronger in Exp4 than that in Exp3 (Figs. 3c, g and k; Figs. 3d, h and l), which suggests that Babuyan Island decreases the Kuroshio transport entering the LS through the Balintany Channel. In addition, Babuyan Island can also affect the cyclonic eddy west of the LS. In winter, the Luzon cold eddy northwest of Luzon Island is clearly stronger in Exp4 than that in Exp3. The former is closer to AVISO satellite altimeter data (Figs. 2a and c).

As shown above, the southern island chain can decrease the westward bending of the Kuroshio path, whereas the middle and north island chain and Babuyan Island can increase the westward bending. All these effects are more remarkable in winter. Furthermore, we find that the addition of the middle and north island chain can result in the occurrence of the Kuroshio east branch, which can be seen clearly in satellite altimeter data. Recently, Sun et al. (2016) found that

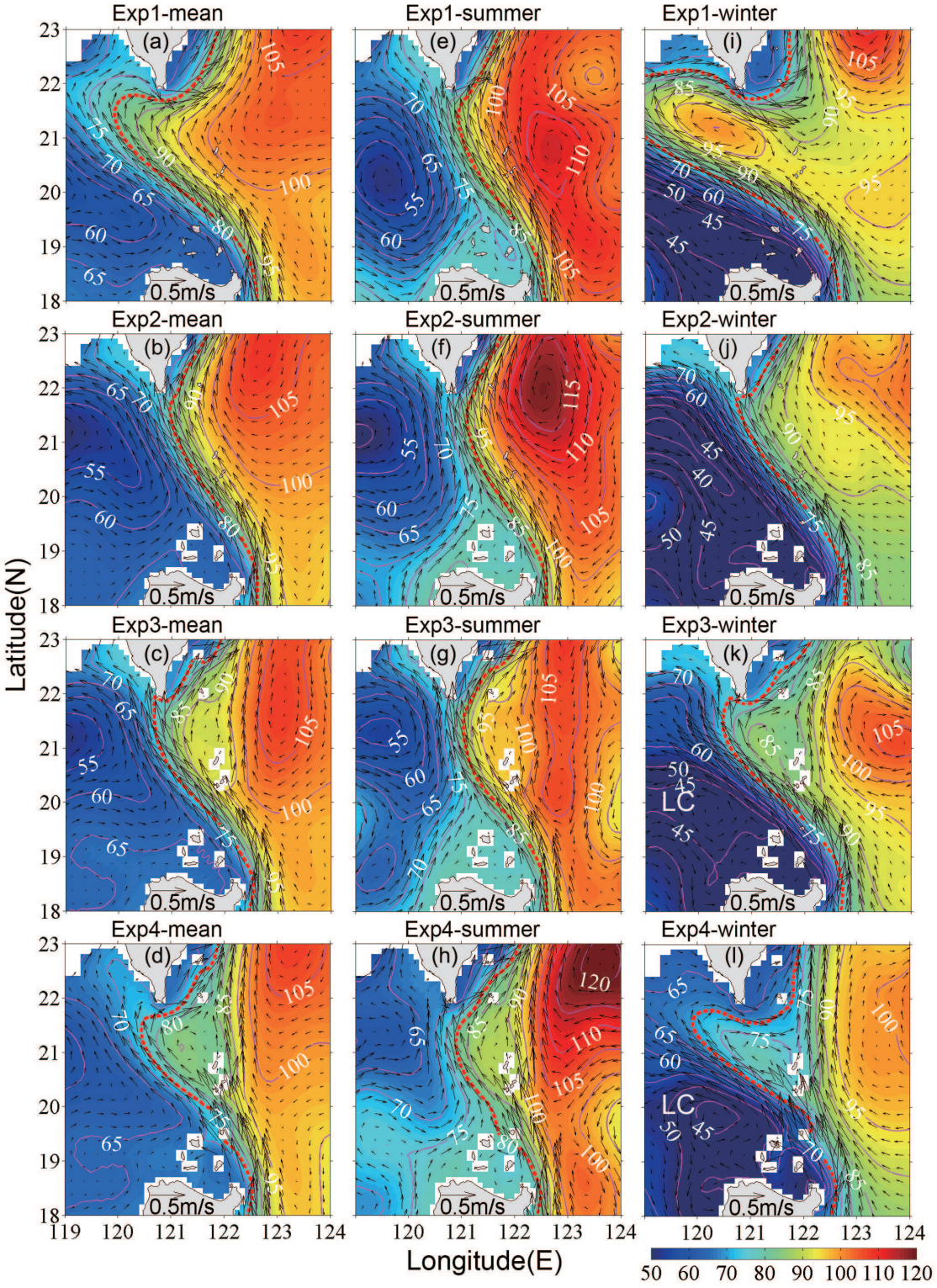

Fig. 3. As in Fig. 2 but for Exp1–Exp4. The red dashed lines represent the Kuroshio paths in the LS. The LCs in panels (k, l) denote the Luzon cold eddy.

the Kuroshio east branch is strongly intensified (weakened) when a warm (cold) eddy approaches the middle island chain from the east. They also suggested that the influence of island chains on the Kuroshio east branch needs to be investigated in the future. Additionally, the island chain topography also has effects on eddies on both sides of the LS. For example, the middle and north island chain can block mesoscale eddies moving from the NWP into the LS, and Babuyan Island has significant influences on the Luzon cold eddy. Interestingly, when all island chains and islands are added, the simulated

SSH and corresponding surface currents are close to satellite altimeter data.

3.2. *SST in winter*

The spatial distribution of SST can also reflect the characteristics of the surface circulation, especially in winter, which is also the season that displays large differences among model experiments. Figure 4a shows the SST in winter (December) for the OISST dataset during 1993–2007, and Figs. 4b–e present the results for Exp1–Exp4. The pink curves highlight both the 25.4°C and 25.6°C isotherms.

The OISST SST shows that two Kuroshio paths are related to high-temperature tongues around the LS: the west tongue extends northwestward from the Balintany Channel to the southwest of Taiwan Island; and the east one extends northward along the east side of the middle and north island chain (Fig. 4a). The 25.4°C isotherm looks like an "M-shape" around the LS. These two tongues correspond to the western and eastern branches of the Kuroshio (Fig. 2c).

Given the absence of a middle and north island chain in the LS, only one Kuroshio high-temperature tongue enters the LS through the Balintany Channel in both Exp1 and Exp2, but Exp2 has less westward tilting than Exp1 (Figs. 4b and c). Obviously, the angle of the westward bending in Exp2 is closer to the observations than that in Exp1. In Exp3, the Kuroshio is split by adding the middle and north island chain; therefore, the two warm water tongues occur (Fig. 4d). However, the SST pattern, the M-shape structure reflected by the 25.6°C or 25.4°C isotherm, is close to the satellite data after adding Babuyan Island in Exp4. These results also indicate that Exp4 can better simulate the path of the Kuroshio in winter than the other three experiments.

A high-temperature tongue extends northward along the west side of Luzon Island (Fig. 4a). However, all the experiments do not reproduce this tongue, and a cold water center is simulated there. This phenomenon may be related to the wind field biases in the CORE2 dataset along the west coast of Luzon Island. As the cold biases cannot significantly affect the role of the island chains in the LS (Fig. 4), we will not investigate the cause of the cold biases further in the present study.

3.3. *Meridional flow*

To further understand the effects of the island chains on the Kuroshio intrusion in the subsurface layer, we select a meridional section across 21.4°N from 119° to 124°E, shown as "AS" in Fig. 2a. Figures 5a, f, and k are the mean, summer, and winter meridional geostrophic velocity (cm s^{-1}), respectively, calculated from the WOA13 temperature and salinity dataset by the geostrophic relationship related to no motion at 1500 m. Figures 5b–e, 5g–j, and 5l–o are the corresponding results for Exp1–Exp4.

Results from the WOA13 dataset show that the maximum of meridional velocity appears between 120.5° and 122.5°E, with values greater than 20 cm s^{-1}, and then gradually decreases from the surface down to the deep ocean. The meridional velocity is strong in summer and weak in winter (Figs. 5f and k). The seasonal variations for the Kuroshio path posi-

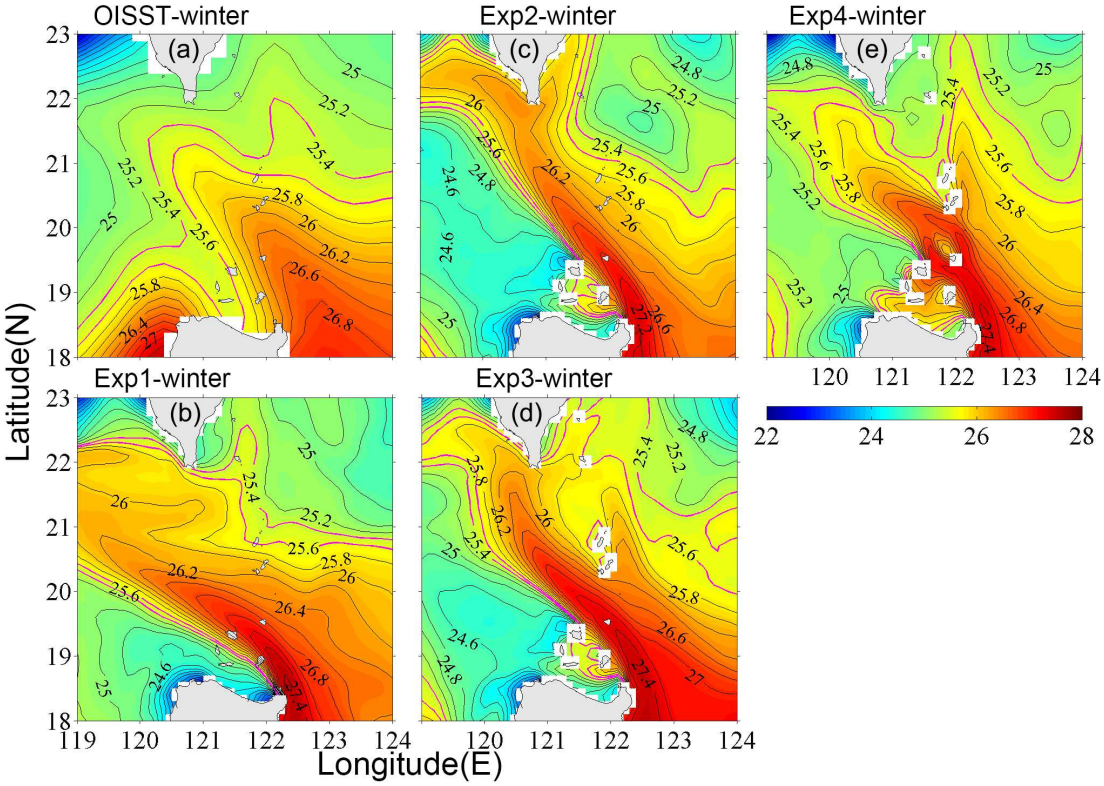

Fig. 4. SST (units: °C) in winter for (a) the OISST dataset and (b–e) Exp1–Exp4. The pink lines highlight the 25.4°C and 25.6°C isotherms.

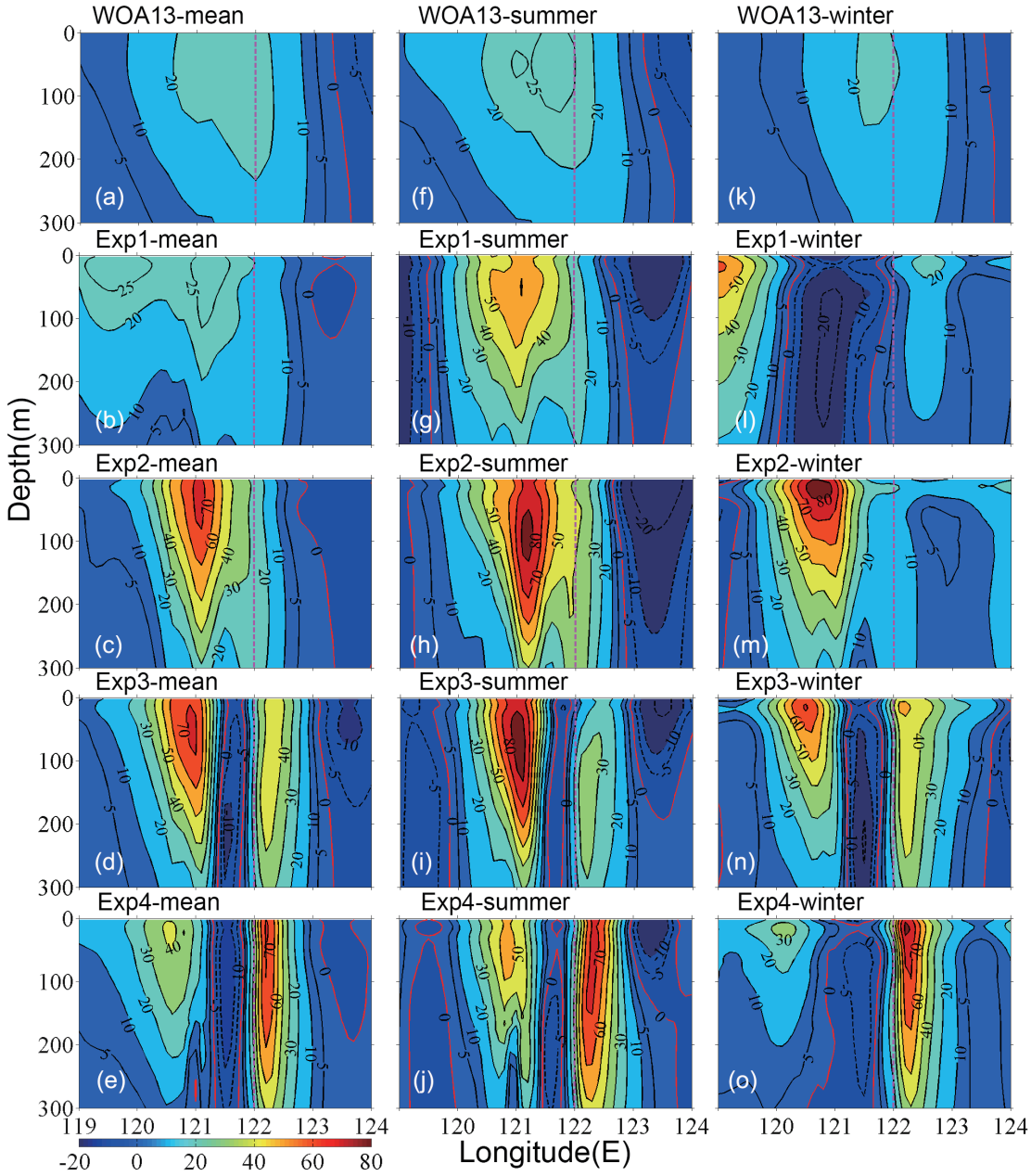

Fig. 5. Geostrophic meridional velocity (units: cm s^{-1}) with a reference level of no motion at 1500 m across the AS section (shown in Fig. 2a): the (a) annual, (f) summer, and (k) winter mean from the WOA13 dataset. Panels (b, g, l), (c, h, m), (d, i, n), and (e, j, o) are the same as (a, f, k) but for Exp1–Exp4, respectively. The black solid (dashed) curves indicate the positive (negative) values denoting northward (southward) flow. The red solid lines denote the contour value of 0. The pink dashed lines denote the location of 122°E.

tion and intensity derived from the WOA13 dataset are consistent with the AVISO observations (Figs. 2b and c). The meridional velocities simulated by Exp1–Exp4 are all greater than the WOA13 dataset in all seasons. In Exp1, two cores of maximum meridional velocity with maximum values larger than 25 cm s^{-1} in the annual mean both occur more westward than that of the WOA13: at 119°–120°E and 121°–122°E (Fig. 5b). These values correspond to the far more westward intrusion of the Kuroshio.

After introducing the south island chain, the maximum meridional velocity in Exp2–Exp4, is primarily between 120.5° and 122.5°E, which is consistent with the results of WOA13. However, model simulations have more complex velocity structures than that of WOA13, especially after introducing the north and middle island chain (Exp3 and Exp4). We find that cores of northward meridional velocity east of 122°E appear in Exp3 and Exp4, which correspond to the east branch of the Kuroshio splitting by the island chain. The Kuroshio east branch is absent from the WOA13 dataset, which may be due to the coarser resolution of WOA13. Differences between Exp3 and Exp4 are also noted. The magnitude of the northward meridional velocity

core west (east) of 122°E decreases (increases) in Exp4 after introducing Babuyan Island. In Exp4, the magnitude of seasonal variation of the maximum meridional velocity east of 122°E becomes small, with maximum values greater than 70 cm s^{-1} in both summer and winter.

Through the analysis of the meridional velocity structures in Exp1–Exp4, we further ensure that both the position and intensity of the Kuroshio path are sensitive to the island chains in the LS. The three zones shown in Fig. 1b have different roles in the Kuroshio intrusion in the LS: the south island chain makes the Kuroshio path shift eastward, the middle and north island chain can split the Kuroshio into two branches, and Babuyan Island can decrease the Kuroshio transport entering the LS and intensify the Kuroshio east branch.

3.4. *Temperature and salinity across the meridional section*

We also investigate the stratification along the aforementioned AS meridional section. The slope of the isotherm can reflect the magnitude and direction of meridional flow. As in Fig. 5, Fig. 6 shows the corresponding temperature along the AS section, with heavy lines highlighting the 17°C isotherm as a reference of the thermocline. The observations from

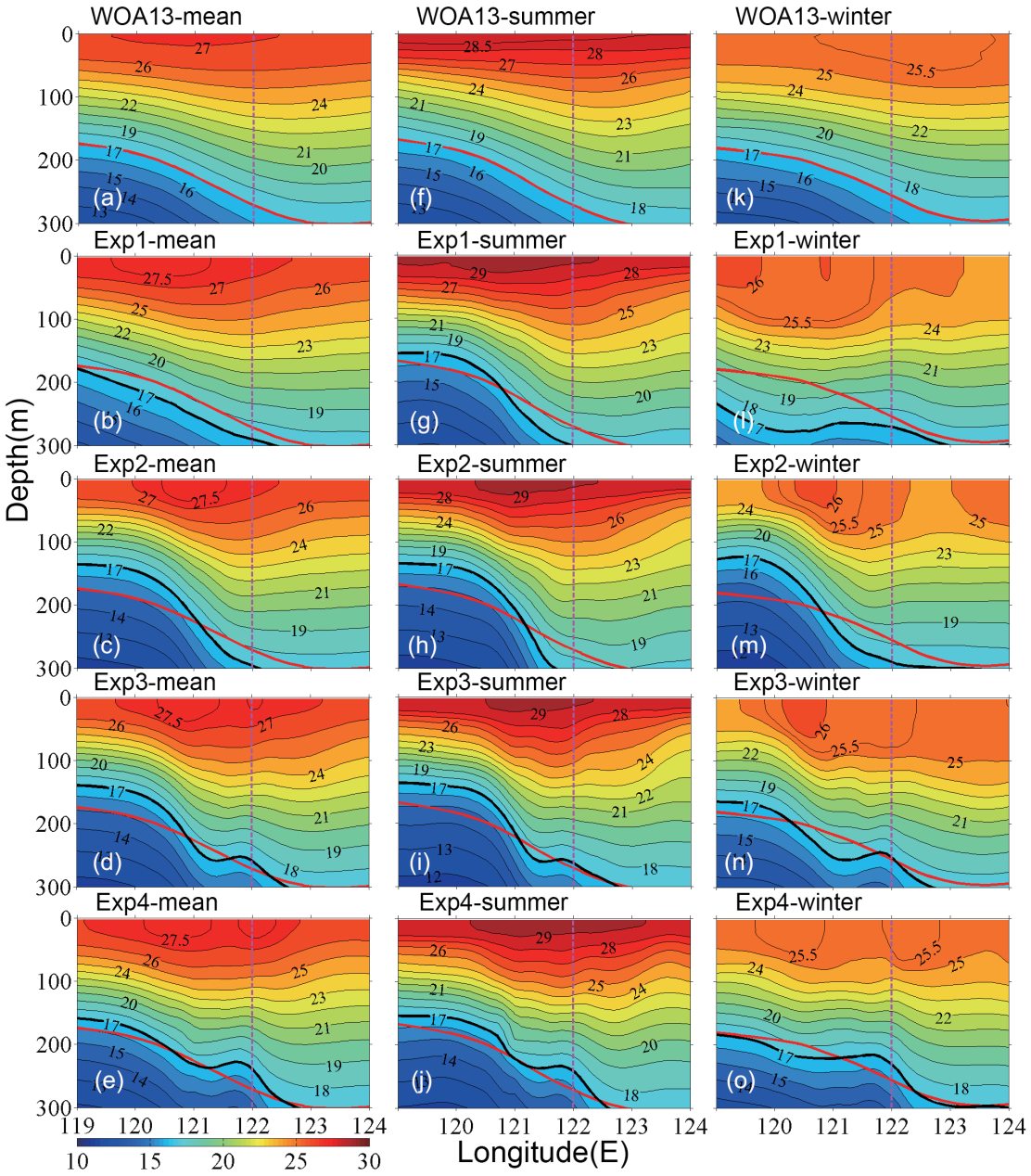

Fig. 6. As in Fig. 5 but for temperature (units: °C). The heavy red curves highlight the 17°C isotherm in the WOA13 dataset, and the heavy black curves indicate the 17°C isotherm for Exp1–Exp4. The pink dashed lines denote the location of 122°E.

WOA13 demonstrate that the 17°C isotherm lines are located between 170 and 300 m and then uplifts from 123°E to west. In Exp1, the annual mean 17°C isotherm is relatively smooth because the Kuroshio intrudes far more westward in the LS in winter (Figs. 6b, g, and l). In Exp2, which includes the south island chain, the gradient of the annual mean 17°C isotherm becomes large compared with the observation between 120.5° and 122.5°E, especially in the annual mean and winter (Figs. 6c, h, and m). In Exp3 and Exp4, in which the middle and north island chain is added, a second large gradient area occurs near 122°E (Figs. 6d, i, and n), which corresponds to the east branch of the Kuroshio. In general, the isotherm slopes are coincident with the meridional flow structures as shown in Fig. 5. The slopes of the isotherms in Exp4 are close to that in observations for the annual mean, summer, and winter, thereby suggesting that the topography in Exp4 is reasonable.

As in Fig. 6, Fig. 7 shows the salinity distribution along the AS section. The 34.70 psu (practical salinity units) isohalines are limited in the east of 120°E for WOA13 (Figs. 7a, f, and k). There is more subsurface high-salinity water extending to the SCS in winter than in summer, which is related to the seasonal variations in the Kuroshio intrusion. The maximum salinity values in these experiments are approximately 0.4 psu lower than the observations. These systematic biases are mainly caused by the surface freshwater biases for

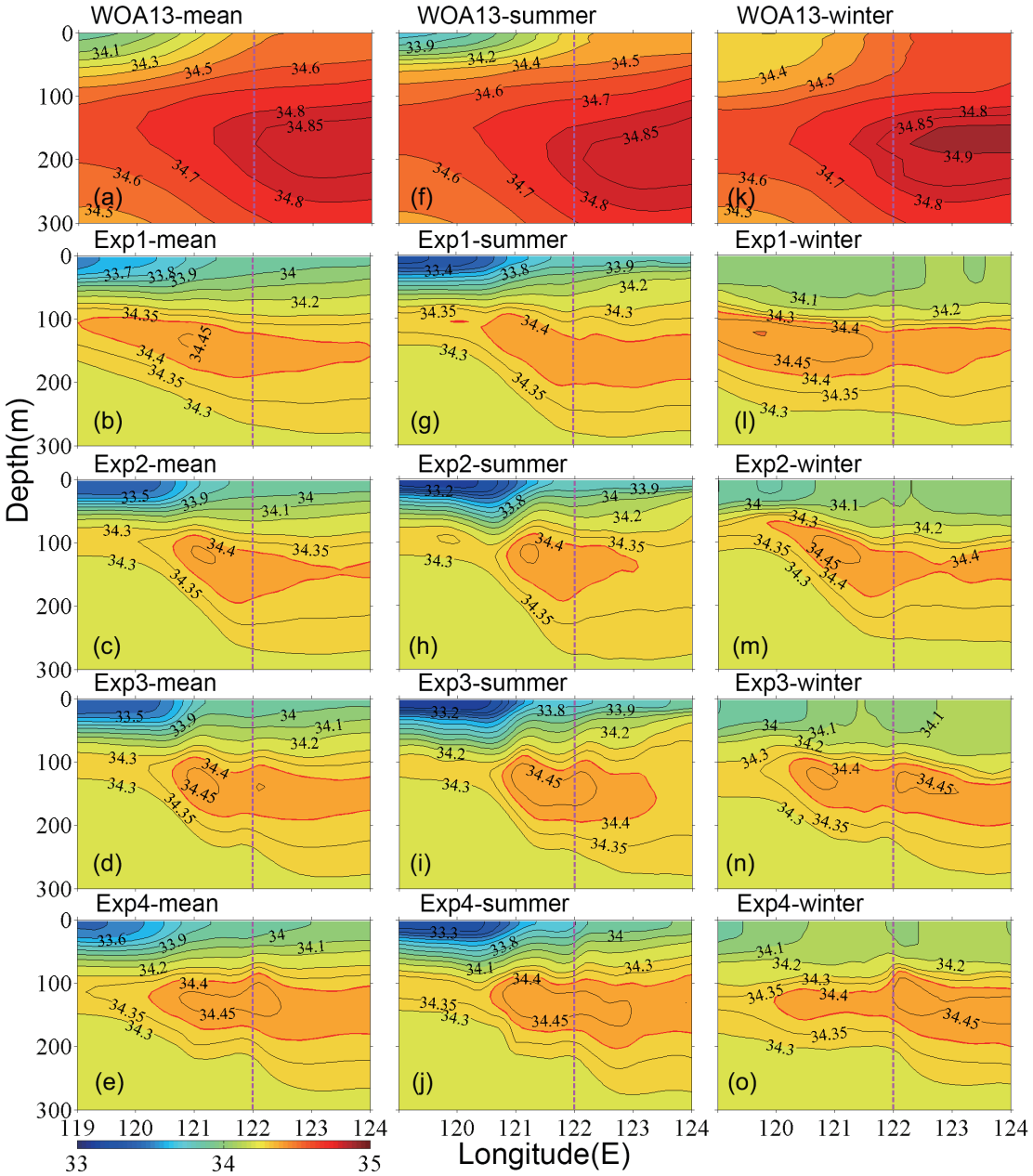

Fig. 7. As in Fig. 5 but for salinity (units: psu). The red curves in panels (b–o) indicate the 34.4 psu isohaline for Exp1–Exp4. The pink dashed lines denote the location of 122°E.

the simulations. In the subsurface layer, the maximum salinity values are between 34.85 and 34.95 psu in WOA13 observations, whereas they are between 34.40 and 34.50 psu in Exp1–Exp4 (highlighted by the red curves). Therefore, we focus on the spatial differences of salinity in the subsurface among Exp1–Exp4, instead of comparing their absolute salinity values with the observations.

Evidently, the annual mean 34.40 psu isohalines in Exp1 intrude farther westward into the northeast SCS than in Exp2–Exp4 (Figs. 7b–e). The most westerly extension of 34.40 psu isohalines occurs in winter when the Kuroshio intrusion is strong. In summer, even in Exp1, the westernmost location of 34.40 psu isohalines is east of 120°E, which is close to the other experiments. When the south island chain is introduced, the westernmost point of the 34.40 psu isohalines in winter is limited to around 120°E. After the middle and north island chain is added, a center of high salinity occurs east of 120°E in winter. Finally, when Babuyan Island is added, the high salinity (34.45 psu isohalines) is limited east of 122°E. These results are all consistent with the variations in the Kuroshio path.

By examining the isotherm slope and the westward extension of the subsurface salinity, we further confirm that the island chains in the LS are important for the Kuroshio intrusion. We also prove that the model topography in Exp4 is relatively close to the observations. Complex isotherm structures exist near island chain topography, indicating the advantages of a high-resolution model in identifying finer spatial structures. Additionally, the causes for salinity biases should be examined in the future.

4. Diagnostic metrics

4.1. *Statistics of Kuroshio intrusion types*

The Double-Index (DI), which is composed of two indices, was proposed by Huang et al. (2016) to describe the spatial patterns of the Kuroshio intrusion and mesoscale eddies west of the LS based on satellite altimeter data. Three typical spatial patterns are identified by the DI: the KWEP, KCEP, and leaking path. In this study, we apply the DI method to compute the occurrence proportions for the Kuroshio intrusion paths in Exp1–Exp4, which allows us to quantitatively assess the influence of island chains on the Kuroshio intrusion.

Figure 8 shows the probabilities of the three kinds of Kuroshio intrusion paths for AVISO and Exp1–Exp4. The satellite altimeter observations suggest that the occurrence proportions for the KWEP, KCEP, and leaking path are 14.1%, 14.8%, and 71.1% during 1993–2013, respectively. In Exp1, the probability of KWEP is 48.4% and much greater than the observations. In Exp2, the main paths are KCEP (29.7%) and leaking path (69.4%), whereas almost no KWEP occurs. These results suggest that the main Kuroshio path leaps the LS or less Kuroshio water flows into the SCS. In Exp3, the probability for KWEP increases to 11.0%, but the probabilities for KCEP and leaking path are 42.5% and 46.5%, respectively. In Exp4, the probabilities for KWEP, KCEP, and leaking path are 14.1%, 8.7%, and 77.2%, respectively, which is the best result among all the experiments.

We also examine the spatial patterns of the three kinds of Kuroshio paths in Exp1–Exp4. These patterns (not shown) are consistent with the corresponding circulation structures given in Fig. 3. As shown above, the effects of the island chains and island can be reflected by the DI, suggesting that the south island chain can efficiently decrease the westward bending of the Kuroshio path. In general, the proportions of the three identified paths also indicate that Exp4 is closest to satellite altimeter observations.

4.2. *Kuroshio transport proportions near the LS*

Besides the Kuroshio flowing through the Balintany Channel, a branch of the Kuroshio flows northward along the east side of the middle and north island chain according to both surface current patterns from AVISO and SST

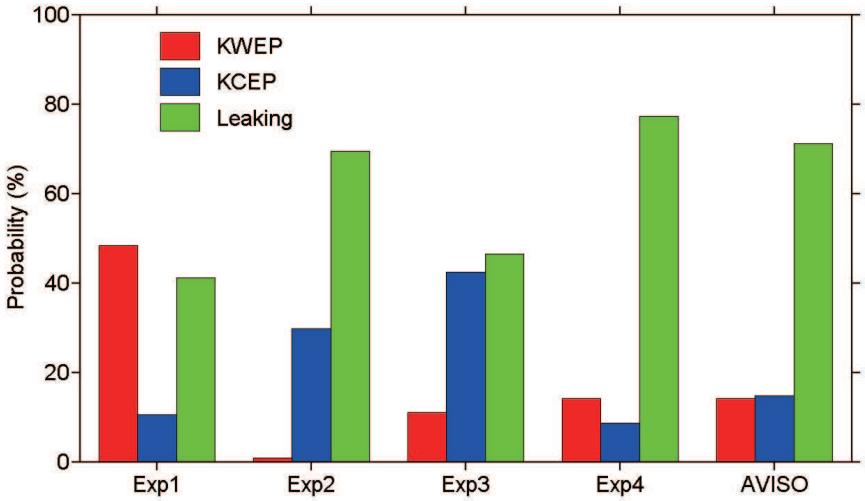

Fig. 8. Occurrence of the Kuroshio intrusion types for AVSIO and Exp1–Exp4. The results of AVISO satellite altimeter data are from Huang et al. (2016).

distributions from OISST. From the abovementioned analysis, the Kuroshio east branch clearly occurs when the middle and north island chain is introduced. Previous studies have presented that the Kuroshio path primarily flows through the Balintany Channel and then enters the LS (Qu, 2000; Nan et al., 2014; Huang et al., 2016). According to mass conservation, the Kuroshio east branch is a part of the Kuroshio, which will reduce the Kuroshio transport through the Balintany Channel. Thus, the quantitative proportion of the Kuroshio transport through the Balintany Channel (or Kuroshio east branch transport) to the total Kuroshio transport can further reveal the sensitivities of the Kuroshio intrusion to island chains.

Given that the water depth is about 1000 m in the Balintany Channel (Figs. 1a and b), we compute the total Kuroshio transport along section S1 in Fig. 9 [(18.3°N, 122.25°–124.0°E), called TS1) and the Balintany Channel transport along section S2 in Fig. 9 [(18.5°–20.4°N, 122.0°E), called TS2] in the upper 1000 m for Exp1–Exp4. The net LSTs are computed along section S3 (18.5°–22.0°N, 120.75°E). Moreover, the Kuroshio east branch transport is difficult to calculate directly because of the effects of complicated circulations and eddies to the east of the LS, so the Kuroshio east branch transport is estimated by TS1–TS2. We also compute the surface (1 m) geostrophic transports from AVISO. In this study, we multiply the transport by 250 for comparison, so we can also consider these values as the transports in the upper 250 m. Given that we are focusing on the partition of transports between the west and east branches, this treatment does not significantly affect the results. The LSTs in Exp1–Exp4 are between 3.7 and 4.3 Sv (Table 2), which fall in the range of the in situ observations and other modeling studies (Tian et al., 2006; Nan et al., 2014).

In AVISO observations, the ratio of TS2 to TS1 is about 68% (Table 2), which suggests that only two-thirds of Kuroshio water flows into the LS through the Balintany Channel. However, nearly 100% of Kuroshio water for Exp1 and Exp2 flows into the LS through the Balintany Channel because of the absence of the Kuroshio east branch. TS2 for Exp1 is even greater than TS1 (Table 2), which suggests that not only all Kuroshio water but also part of the water from North Pacific flows into the LS. When the middle and north island chain is added, the ratio of TS2 to TS1 decreases significantly by about 82% for Exp3 and 60% for Exp4, respectively. The ratio in the latter (Exp4) is closer to that in the satellite altimeter observations.

East of the middle and north island chain, the "east" branch comprises the Kuroshio east branch and the recirculation cell. The transport of the recirculation (TR) is defined as the transport of S4 (20.4°N, 120°–124°E) + S2 (18.5°–

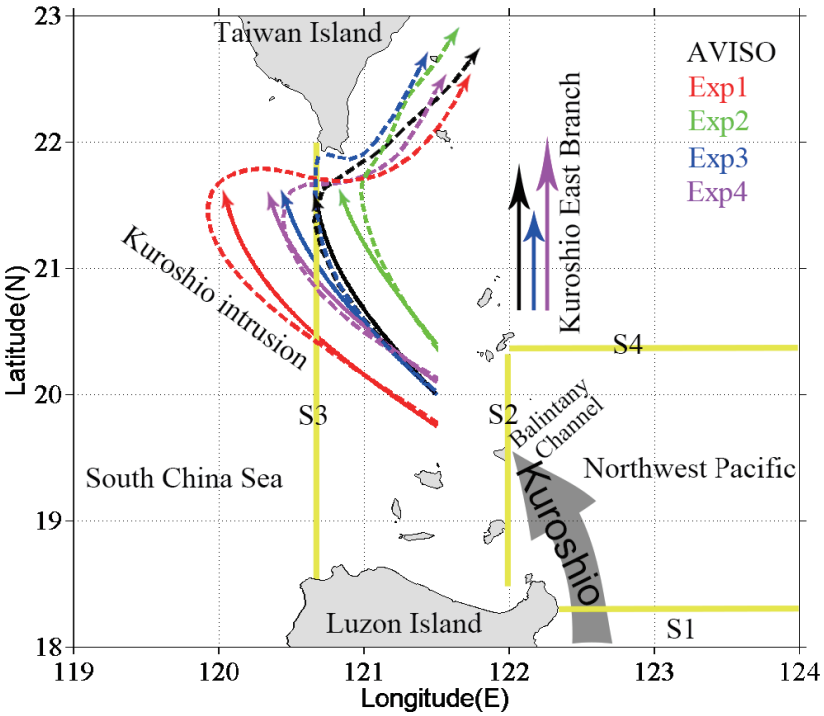

Fig. 9. Diagram of the Kuroshio paths in the LS. The dashed lines represent the Kuroshio paths in the LS for AVSIO and Exp1–Exp4 (Figs. 2a and 3a–d). The solid lines are calculated from the conservation of the absolute vortices [Eq. (1)] of Li and Liu (1997). All the dynamic parameters are listed in Table 3. The vectors east of the LS denote the Kuroshio east branch. The yellow lines, S1 (18.3°N, 122.25°–124.0°E), S2 (18.5°–20.4°N, 122.0°E), S3 (18.5°–22.0°N, 120.75°E), and S4 (20.4°N, 120.0°–124.0°E,) are sections for computing the volume transports in Table 2.

Table 2. The upper 1000 m volume transports along sections S1, S2 and S4, as shown in Fig. 9, for AVISO and Exp1–Exp4 [Sv (Sv, 10^6 m^3 s^{-1})]. Section S3 is used to calculate the net Luzon Strait Transport (LST). Here, we use the total Kuroshio transport minus the Balintany Channel transport ($TS_1 - TS_2$) to compute the transport of the east branch of the Kuroshio. The transport of the recirculation is defined by the transport of ($TS_4 + TS_2 - TS_1$). The water depth for calculating the transports is 250 m for AVISO.

	LST	TS1	TS2	$TS_1 - TS_2$	TS_2/TS_1 (100%)	TS_4	TR	TR/TS_4 (100%)
AVISO	3.7	16.4	11.2	4.8	68%	4.8	0	0%
Exp1	4.3	19.0	20.5	−1.5	108%	—	—	—
Exp2	4.1	16.9	16.9	0.0	100%	—	—	—
Exp3	4.1	18.7	15.4	3.3	82%	9.5	6.2	65%
Exp4	3.7	16.8	10.0	6.8	60%	13.2	6.4	48%

20.4°N, 122.0°E) − S1 (18.3°N, 122.25°–124.0°E). After calculation, the ratios of the Kuroshio east branch (recirculation) to the "east" branch are 100% (0%) in AVISO data, 35% (65%) in Exp3, and 52% (48%) in Exp4 (Table 2). It is worth noting that the TR is sensitive to the selection of the section, because the positions and sizes of the recirculation cells are different among these data.

4.3. *Westward bending of the mean main Kuroshio path*

Based on vorticity conservation, work has been conducted on the dynamic mechanisms for Kuroshio deformations in the LS (Li and Liu, 1997; Sheremet, 2001; Yuan and Wang, 2011). The Kuroshio path in the LS, which loses support from the western boundary, can be regarded as an inertial jet flow following the absolute vorticity conservation equation. Assuming geostrophic balance, β plane approximation, and frictionless flow, the Kuroshio path can be expressed as follows (Li and Liu, 1997):

$$y = \left[2(\cos\theta - \cos\theta_0)\frac{V_c}{\beta}\right]^{\frac{1}{2}}, \quad (1)$$

where β is the variation in the Coriolis parameter with latitude and approximately equal to 2.0×10^{-11} m^{-1} s^{-1}; and V_c and θ_0 are the inflow speed and incidence angle for the core of the Kuroshio path when entering the LS, respectively. θ is measured anticlockwise from the east. From Eq. (1), the increase in both V_c and θ_0 will intensify the westward bending of the main Kuroshio path, so the relationships between westward bending and island chains can be discussed quantitatively.

As mentioned in section 3.1, the mean Kuroshio paths are extracted from the SSH values with 115 cm for observations, 80 cm for Exp1 and Exp2, and 75 cm for Exp3 and Exp4 (red dashed contours in Figs. 2a and 3). By selecting 121.5°E as the initial longitude in these SSH contours, we obtain the initial latitude, inflow speed V_c, and incidence angle θ_0. These dynamic parameters for the AVISO and all experiments are listed in Table 3. Figure 9 demonstrates the Kuroshio paths in the LS for the model simulations (the dashed curves) and for the results from Eq. (1) (the solid curves). No significant distinction is found between the solid and dashed curves in observations and each experiment as shown in Fig. 9. Therefore, we can use this relation to analyze the effects of the island chains or island on the Kuroshio path.

Exp1 and Exp2 have the same value of V_c (0.72 m s^{-1}) but different values of θ_0; namely, 140° for Exp1 and 123° for Exp2. Clearly, the mean Kuroshio path is mainly in a state of looping for Exp1 but in a state of leaping for Exp2, because of the small incidence angle in Exp2. These findings reveal that the south island chain reduces the westward bending of the Kuroshio by decreasing θ_0. The incidence angle decrease from Exp1 to Exp2 is caused by adding the solid boundary support of the south island chain. Meanwhile, the incidence angle increase from Exp2 to Exp3 is caused by the splitting effect of the middle and north island chain; the left (right) of the Kuroshio shifts westward (northward) and forms the Kuroshio west (east) branch. Similarly, the splitting effect of the Babuyan Island results in the increase of the incidence angle from Exp3 to Exp4. In Exp3, both θ_0 and V_c for Exp3 increase to 131° and 0.79 m s^{-1}, respectively, which both increase the westward bending of the Kuroshio path. After introducing Babuyan Island (Exp4), θ_0 is further increased to 138°, but V_c is decreased to 0.53 m s^{-1}. This phenomenon leads to slightly more westward bending of the Kuroshio than that for Exp3. Notably, the westward bending of the Kuroshio path increases from Exp2 to Exp4 (Table 3), but primarily in a state of leaping, which are all close to the satellite altimeter observations.

Table 3. Initial positions and dynamic parameters (V_c, θ_0) for AVISO and Exp1–Exp4.

	Initial position (°N, °E)	Inflow speed (V_c, m s^{-1})	Incidence angle (θ_0)	Westernmost point at 21.5°N
AVISO	(20.0, 121.5)	0.62	127°	120.70°E
Exp1	(19.7, 121.5)	0.72	140°	120.05°E
Exp2	(20.4, 121.5)	0.72	123°	120.85°E
Exp3	(20.0, 121.5)	0.79	131°	120.45°E
Exp4	(20.1, 121.5)	0.53	138°	120.35°E

The relationship between the westward bending of the Kuroshio and the incidence angle, θ_0, as well as the inflow speed, V_c, is investigated in the present subsection. As in previous studies, increasing θ_0 and V_c will increase the westward bending of the Kuroshio. The model results are similar to the idealized relationship. Evidently, the south island chain changes the Kuroshio intrusion through the change in θ_0, the middle and north island chain also through the change in θ_0, and Babuyan Island through the change in both θ_0 and V_c. Based on Exp2–Exp4, the westward bending of the Kuroshio path increases with the increase in the inflow angle, accompa-

nied by less Kuroshio water flowing into the LS, as shown in subsection 4.2. These results are consistent with the β effect (Sheremet, 2001; Wang et al., 2006).

5. Summary

By applying a global high-resolution (0.1°) OGCM, LICOM2.0, we study the effects of the island chains in the LS on the Kuroshio intrusion. The island chains in the LS are separated into three parts: the south island chain, the middle and north island chain, and Babuyan Island. One control and three sensitivity experiments are conducted by adding a chain of three islands or each island gradually. Through comparisons of the circulation, temperature, and salinity structures, the roles of these three parts of the islands are well presented. Furthermore, analyses of the Kuroshio intrusion path proportions and the Kuroshio transport proportions, and dynamic diagnoses, are performed to understand how the island chains affect the Kuroshio deformations in the LS.

Analyses demonstrate that island chains have significant effects on the main Kuroshio path in the LS. The south island chain decreases the westward bending of the main Kuroshio path, the middle and north island chain increases the westward bending, and Babuyan Island also increases the westward bending. These results are extremely clear in winter. Dynamic diagnoses using the method of Li and Liu (1997) suggest that the westward bending increases with an increase in the incidence angle of the Kuroshio, a decrease in the Kuroshio transport into the LS, and an increase in the Kuroshio east branch transport. Moreover, the middle and north island chain can split the Kuroshio into two parts: the Kuroshio west and east branches, which can also be seen clearly in the satellite altimeter maps.

As shown above, the Kuroshio intrusion is sensitive to islands in the LS. These results also reflect the importance of increasing the model resolution to resolve these islands. These conclusions are consistent with the study of Metzger and Hurlburt (2001). Additionally, there are significant SST biases west of Luzon Island, even if all island chains and islands are considered in Exp4. These biases may come from other processes, such as the forcing data. These biases will be investigated in the future.

Acknowledgements. This work was supported by the National Basic Research Program of China (Grant Nos. 2015CB954004 and 2013CB956204), the Strategic Priority Research Program (Grant No. XDA11010304) entitled "Western Pacific Ocean System: Structure, Dynamics and Consequences" of the Chinese Academy of Sciences, and the National Natural Science Foundation of China (Grant Nos. 41276006, U1405233, 41576025 and 41576026). We appreciate the online data from AVISO, OISST, and WOA13.

REFERENCES

Caruso, M. J., G. G. Gawarkiewicz, and R. C. Beardsley, 2006: Interannual variability of the Kuroshio intrusion in the South China Sea. *Journal of Oceanography*, **62**, 559–575.

Hu, J. Y., H. Kawamura, H. S. Hong, and Y. Q. Qi, 2000: A review on the currents in the South China Sea: Seasonal circulation, South China Sea Warm Current and Kuroshio intrusion. *Journal of Oceanography*, **56**, 607–624.

Hu, J. Y., J. Y. Pan, X. Y. Gou, and Q. A. Zheng, 2011: Introduction to the special section on regional environmental oceanography in the South China Sea and its adjacent areas (REO-SCS): I. *Journal of Oceanography*, **67**, 359–363, doi: 10.1007/s10872-011-0063-y.

Hu, J. Y., Q. A. Zheng, Z. Y. Sun, and C.-K. Tai, 2012: Penetration of nonlinear Rossby eddies into South China Sea evidenced by cruise data. *J. Geophys. Res.*, **117**, C03010, doi: 10.1029/2011JC007525.

Huang, Z. D., H. L. Liu, J. Y. Hu, and P. F. Lin, 2016: A double-index method to classify Kuroshio intrusion paths in the Luzon Strait. *Adv. Atmos. Sci.*, **33**(6), 715–729, doi: 10.1007/s00376-015-5171-y.

Lan, J., X. W. Bao, and G. P. Gao, 2004: Optimal estimation of zonal velocity and transport through Luzon Strait using variational data assimilation technique. *Chinese Journal of Oceanology and Limnology*, **22**, 335–339.

Li, L., W. D. Nowlin Jr., and J. L. Su, 1998: Anticyclonic rings from the Kuroshio in the South China Sea. *Deep Sea Research Part I*: *Oceanographic Research Papers*, **45**, 1469–1482, doi: 10.1016/S0967-0637(98)00026-0.

Li, W., and Q. Y. Liu, 1997: A preliminary study of the deformation and its dynamics of western boundary current at a gap. *Journal of Ocean University of Qingdao*, **27**(3), 277–281. (in Chinese)

Liu, H. L., X. H. Zhang, W. Li, Y. Q. Yu, and R. C. Yu, 2004: An eddy-permitting oceanic general circulation model and its preliminary evaluation. *Adv. Atmos. Sci*., **21**, 675–690, doi: 10.1007/BF02916365.

Liu, H. L., P. F. Lin, Y. Q. Yu, and X. H. Zhang, 2012: The baseline evaluation of LASG/IAP Climate system Ocean Model (LICOM) version 2. *Acta Meteorologica Sinica*, **26**(3), 318–329, doi: 10.1007/s13351-012-0305-y.

Lu, J. Y., and Q. Y. Liu, 2013: Gap-leaping Kuroshio and blocking westward-propagating Rossby wave and eddy in the Luzon Strait. *J. Geophys. Res.*, **118**, 1170–1181, doi: 10.1002/jgrc.20116.

Metzger, E. J., and H. E. Hurlburt, 2001: The importance of high horizontal resolution and accurate coastline geometry in modeling South China Sea inflow. *Geophys. Res. Lett.*, **28**, 1059–1062.

Nan, F., H. J. Xue, and F. Yu, 2014: Kuroshio intrusion into the South China Sea: A review. *Progress in Oceanography*, **137**, 314–333, doi: 10.1016/j.pocean.2014.05.012.

Qu, T. D., 2000: Upper-layer circulation in the South China Sea. *Journal of Physical Oceanography*, **30**, 1450–1460.

Sheremet, V. A., 2001: Hysteresis of a western boundary current leaping across a gap. *Journal of Physical Oceanography*, **31**, 1247–1259.

Shu, Y. Q., H. J. Xue, D. X. Wang, F. Chai, Q. Xie, J. L. Yao, and J. G. Xiao, 2014: Meridional overturning circulation in the South China Sea envisioned from the high-resolution global reanalysis data GLBa0.08. *J. Geophys. Res.*, **119**, 3012–3028. doi: 10.1002/2013JC009583.

Sun, R. L., G. H. Wang, and C. L. Chen, 2016: The Kuroshio bifurcation associated with islands at the Luzon Strait. *Geophys. Res. Lett.*, **43**, doi: 10.1002/2016GL069652.

Tian, J. W., Q. X. Yang, X. F. Liang, L. L. Xie, D. X. Hu, F.

Wang, and T. D. Qu, 2006: Observation of Luzon Strait transport. *Geophys. Res. Lett.*, **33**, L19607, doi: 10.1029/2006GL026272.

Wang, D. X., Q. Y. Liu, R. X. Huang, Y. Du, and T. D. Qu, 2006: Interannual variability of the South China Sea throughflow inferred from wind data and an ocean data assimilation product. *Geophys. Res. Lett.*, **33**, L14605, doi: 10.1029/2006GL026316.

Yu, Y. Q., H. L. Liu, and P. F. Lin, 2012: A quasi-global 1/10° eddy-resolving ocean general circulation model and its preliminary results. *Chinese Science Bulletin*, **57**, 3908–3916, doi: 10.1007/s11434-012-5234-8.

Yuan, D. L., and Z. Wang, 2011: Hysteresis and dynamics of a western boundary current flowing by a gap forced by impingement of mesoscale eddies. *J. Phys. Oceanogr.*, **41**, 878–888, doi: 10.1175/2010JPO4489.1.

Zheng, Q. A., H. Lin, J. M. Meng, X. M. Hu, Y. T. Song, Y. Z. Zhang, and C. Y. Li, 2008: Sub-mesoscale ocean vortex trains in the Luzon Strait. *J. Geophys. Res.*, **113**, C04032，doi: 10.1029/2007JC004362.

Zheng, Q. A., C. K. Tai, J. Y. Hu, H. Y. Lin, R. H. Zhang, F. C. Su, and X. F. Yang, 2011: Satellite altimeter observations of nonlinear Rossby eddy–Kuroshio interaction at the Luzon Strait. *J. Oceanogr.*, **67**, 365–376, doi: 10.1007/s10872-011-0035-2.